Journal of Contaminant Hydrology 250 (2022) 104054

Contents lists available at ScienceDirect

Journal of Contaminant Hydrology

journal homepage: www.elsevier.com/locate/jconhyd

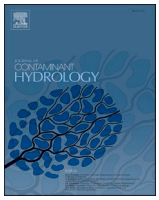

Evaluating low-cost permeable adsorptive barriers for the removal of benzene from groundwater: Laboratory experiments and numerical modelling

Franklin Obiri-Nyarko [a,*], Jolanta Kwiatkowska-Malina [b], Samuel Kwame Kumahor [c], Grzegorz Malina [d]

[a] Groundwater Division, CSIR-Water Research Institute, P. O. Box M 32, Accra, Ghana
[b] Department of Spatial Planning and Environmental Sciences, Faculty of Geodesy and Cartography, Warsaw University of Technology, Pl Politechniki 1, 00-661 Warsaw, Poland
[c] Department of Soil Science, University of Ghana, P.O. Box LG 25, Legon, Ghana
[d] Department of Hydrogeology and Engineering, Geology AGH University of Science and Technology, Al. Mickiewicza 30, 30-059 Krakow, Poland

ARTICLE INFO

Keywords:
Permeable sorption barrier
Compost
Brown coal
Zeolite
Benzene
Analytical modelling

ABSTRACT

Permeable adsorptive barriers (PABs) consisting of individual (compost, zeolite, and brown coal) and composite (brown coal-compost and zeolite-compost) adsorbents were evaluated for their hydraulic performance and effectiveness in removing aqueous benzene using batch and column experiments. Different adsorption isotherms and kinetic models and different formulations of the equilibrium advection-dispersion equation (ADE) were evaluated for their capabilities to describe the benzene sorption in the media. The batch experiments showed that the adsorption of benzene by the adsorbents was favourable and could be adequately described by the Freundlich and Langmuir isotherms and the pseudo-second-order kinetic model. Particle attrition and structural reorganization occurred in the columns, possibly introducing preferential flow paths and resulting in slight changes in the final hydraulic conductivity values (4.3×10^{-5} cm s^{-1}–1.7×10^{-3} cm s^{-1}) relative to the initial values (4.2×10^{-5} cm s^{-1}–2.14×10^{-3} cm s^{-1}). Despite the fact that preferential flow appeared to have an impact on the performance of the investigated adsorbents, the brown coal-compost mixture proved to be the most effective adsorbent. It significantly delayed benzene breakthrough ($R = 29$), indicating that it can be applied as a low-cost effective adsorbent in PABs for sustainable remediation of benzene-contaminated groundwater. The formulated transport models could fairly describe the behaviour of benzene in the investigated media under dynamic flow conditions; however, model refinement and additional experimental studies are needed before pilot/full-scale applications to improve the fits and verify the benzene removal processes. Our results generally demonstrate how such studies can be useful in evaluating potential reactive barrier materials.

1. Introduction

Benzene (C_6H_6) is a naturally occurring volatile organic compound (VOC) and one of the contaminants commonly found in groundwater worldwide. Its occurrence in groundwater is often due to underground leaks and surface spills of petroleum products (Liu et al., 2010). High amounts of benzene exposure in humans via consumption of groundwater can cause serious health problems such as cancer, mucosal irritation, haematological abnormalities, permanent damage to the central nervous system, respiratory issues, and liver and kidney disorders (Liang and Chen, 2010; Bahadar et al., 2014). As a result, its removal from environmental systems is necessary to avoid these health issues.

Among the existing groundwater remediation methods, the permeable reactive barrier (PRB) technology has gained popularity in recent times because it is relatively cheap and can be used to remove a wide variety of contaminants, including heavy metals (e.g., lead, cadmium, and arsenic), chlorinated solvents (e.g., tri- and tetra- chloroethylenes), petroleum hydrocarbons (e.g., benzene, toluene, ethylbenzene, and xylene) and nutrients (e.g., phosphorus and nitrate) from groundwater (Obiri-Nyarko et al., 2014). The PRB technology generally involves the

* Corresponding author.
E-mail addresses: fobiri-nyarko@csir.org.gh (F. Obiri-Nyarko), jolanta.kwiatkowska@pw.edu.pl (J. Kwiatkowska-Malina), skumahor@ug.edu.gh (S.K. Kumahor), gmalina@agh.edu.pl (G. Malina).

https://doi.org/10.1016/j.jconhyd.2022.104054
Received 24 January 2022; Received in revised form 19 July 2022; Accepted 23 July 2022
Available online 28 July 2022

emplacement of a barrier filled with a reactive material(s) across the flow trajectory of the contaminant plume. As the contaminated groundwater flows passively through the barrier under the influence of the natural hydraulic gradient, the contaminants are removed (via mechanisms such as sorption, biodegradation, ion exchange, precipitation, etc.), allowing treated groundwater to emerge downstream of the barrier (Henderson and Demond, 2007; Obiri-Nyarko et al., 2014). Several forms/designs of the PRB technology have emerged since its inception, and these are based on factors such as the employed removal processes and the nature of the contamination. Some variants include permeable sorption barrier (PSB), permeable adsorptive barrier (PAB), permeable reactive bio-barriers (PRbB), and permeable reactive multi-barrier (PRmB) (Erto et al., 2011; Obiri-Nyarko et al., 2014; Freidman et al., 2017; Zawierucha and Nowik-Zajac, 2019).

In PRBs, adsorption is one of the mechanisms commonly used to remove organic compounds such as benzene from groundwater. This owes to the fact that it allows the utilization of a wide spectrum of adsorbents, including natural and synthetic materials, as well as low-cost and eco-friendly waste materials and by-products (e.g., Simpson and Bowman, 2009; Faisal et al., 2021). Moreover, adsorption has proven to be highly efficient for removing contaminants at low concentrations (Simantiraki and Gidarakos, 2015). Furthermore, the adsorption process does not produce detrimental derivatives and also allows the recovery of the used adsorbent (Erto et al., 2010). So far, different adsorbents have been tested with different removal efficiencies and adsorption characteristics. Faisal et al. (2021) studied benzene adsorption in a cement kiln dust (CKD)-PRB and found a non-linear sorptive behaviour of benzene, which was best described by the Langmuir isotherm and the pseudo-first-order (PFO) kinetic model. They also attributed the adsorption of benzene by the CKD to electrostatic interaction between the adsorbent and benzene. Suponik (2010) reported that the adsorption of benzene onto granular activated carbon (GAC) largely obeyed the Freundlich isotherm. The adsorption of Benzene, Toluene, Ethylbenzene, and Xylene (BTEX) in a natural zeolite-PRB was also studied by Vaezihir et al. (2020). They noted that the barrier efficiency started to decline after 132 h due to the occupation of the adsorption sites by the BTEX molecules. Vignola et al. (2011) also reported an excellent adsorption efficiency (96%) for BTEX in a surfactant modified zeolite (ZSM-5)-PRB. Due to the generally high cost of some of these adsorbents, efforts are being made to identify/develop low-cost substitutes, preferably eco-friendly waste materials and by-products.

Many studies have shown that the operational life of the PRB can be truncated, owing to early exhaustion of the capacity or passivation-induced loss of the reactive medium (Kamolpornwijit et al., 2003; Obiri-Nyarko et al., 2014; Yang et al., 2021). Some researchers have also reported changes in the pore geometry (i.e. increase or reduction of porosity) due to reorganization of grains by the infiltrating solution, dissolution/degradation of media, biofouling or production of secondary products during PRB operation (e.g., Eykholt et al., 1999; Kamolpornwijit et al., 2003; Henderson and Demond, 2007; Vignola et al., 2011). Obiri-Nyarko et al. (2014) reviewed reactive materials used in PRBs and noted that when mixtures of materials are used, they sometimes tend to show antagonistic (inhibitory) instead of synergistic (stimulatory) effects. Given the above issues, it is imperative to thoroughly assess proposed reactive materials for their effectiveness and to identify possible issues that can affect the performance of the PRB before field-scale application.

The use of laboratory-scale experiments (batch and column) to evaluate reactive materials for PRBs is common (e.g., Waybrant et al., 2002; Chen et al., 2011; Obiri-Nyarko et al., 2020; Faisal et al., 2021). Batch tests are used for screening whereas column experiments allow the applicability of the materials to be assessed under simulated field conditions (Waybrant et al., 2002). For instance, the fate and transport of contaminants in PRBs as well as the hydraulic performance of reactive materials can be studied concurrently using column techniques (Bilardi et al., 2016; Obiri-Nyarko et al., 2020). In some cases, mathematical/numerical modelling has been performed to predict the long-term performance of PRBs, aid the evaluation of the materials and the design of the PRB as well as elucidate the contaminant removal mechanisms. For example, Rabideau et al. (2005) employed the advective-dispersive-reactive equation (ADRE) with a zero concentration gradient imposed on the exit boundary of the PRB to determine the PRB thickness. Obiri-Nyarko et al. (2015) performed geochemical modelling using PHREEQC to predict the long-term performance of a zeolite-PRB to treat lead-contaminated groundwater. A numerical model based on Visual MODFLOW was also developed to evaluate: (i) flow changes due to the installation of diverse PRB systems to propose the optimum configuration, length and thickness, and (ii) impacts of changes in the reactive material's hydraulic conductivity overtime on key design parameters: capture zone, residence time and discharge rate (Grajales-Mesa et al., 2020). Yang et al. (2021) also recently developed a mathematical model based on Faraday's law, which integrates iron surface passivation to describe the porosity change of a hypothetical Fe^0-based PRB. Most of these models are based on the classical advection-dispersion equation (ADE), which assumes instantaneous sorption and a constant dispersivity, irrespective of the travel distance (Mahdipanah et al., 2022).

In the present study, low-cost adsorbents including compost, natural zeolite, and brown coal as well as their mixtures were evaluated as PABs for the removal of benzene from groundwater. Although some of these sorbents have been studied individually, their mixtures have neither been assessed in a single PAB nor under dynamic conditions. We hypothesized that the combination of some of these materials may lead to improved removal efficiency and hydraulic performance of the PAB. Batch tests were initially conducted to analyze the individual materials, followed by column studies to evaluate the reactivity of the materials (individual as well as their mixtures) and their hydraulic characteristics. The applicability of two analytical solutions of the ADE to describe benzene behaviour in the investigated media was also evaluated.

2. Materials and methods

2.1. Reactive materials

Compost was obtained from food and plant waste while brown coal was acquired from a lignite opencast depot located at Konin, Poland. Zeolite was obtained from a private company in Poland and contained a substantial (75%) content of clinoptilolite. Other properties of the studied materials are reported in Table 1. Briefly, the pH of the materials was determined in water (1 part of the material to 2.5 parts of water) using a multifunctional computer meter (Elmetron Cx-742) while the gravimetric method (Topp, 1993) was applied for the moisture content (MC) determination based on Eq. (1):

$$MC\% = \frac{M_W}{M_{DS}} \times 100 \quad (1)$$

where: M_w (g): mass of water = M_{ws} (mass of moist material) – M_{Ds} (mass of dry solid); M_{DS} (g): mass of dry solid = (mass of moisture can + dried material) – (mass of clean moisture can).

The bulk density (ρ_b) of the materials was determined using Eq. (2).

Table 1
Physico-chemical properties of the studied materials.

Parameters	Materials		
	Zeolite	Compost	Brown coal
$pH_{(H2O)}$	7.13	8.05	4.90
ρ_b (g cm^{-3})	0.80	0.69	1.13
CEC [mmol(+) kg^{-1}]	435.5	480.0	1215.0
Grain size (mm)	2.0–2.5	1.0–2.5	0.2–0.5
f_{oc} (%)	0.03	0.20	0.17

ρ_b: bulk density; CEC: cation exchange capacity; f_{oc}: fraction of organic carbon; and MC: moisture content.

The samples were poured into a cylindrical glass with known volume, V_b (cm^3), and weight, C_m (g). M_b (g) represents the weight of the cylindrical glass filled with the material (Al-Shammary et al., 2018).

$$\rho_b = \frac{M_b - C_m}{V_b} \quad (2)$$

The protocol described by Thorpe (1973) was employed to determine the cation exchange capacity (CEC) of the materials. Two (2) g of each sample was soaked in 100 mL 0.5 N HCl for H^+ to displace the cations in the materials. Thereafter, the samples were soaked in 100 mL of barium acetate [0.5 N $Ba(OAc)_2$] to displace the H^+ by saturating the exchange sites with barium (Ba^{2+}). The suspension was filtered and the samples were washed with water. The combined $Ba(OAc)_2$ filtrate + wash filtrates solution was titrated with sodium hydroxide (0.1 N NaOH) to a phenolphthalein endpoint (pH ≈ 8.0). The CEC was calculated from the number of moles of the NaOH consumed. The fraction of organic carbon (f_{oc}) was calculated from the organic carbon (OC) content of the samples, which was determined using the loss-on-ignition (LOI) method. This method estimates organic matter (OM) based on a gravimetric weight change associated with high-temperature oxidation of OM. In the present study, the samples were initially oven-dried at 105 °C, after which they were ignited in a muffle furnace at 450 °C for 4 h. The per cent weight loss represented the OM-LOI (% wt. loss), which was converted to OC using the van Bemmelen factor of 1.724 (Sutherland, 1998; Wright et al., 2008).

2.2. Batch adsorption isotherms and kinetics experiments

Batch adsorption experiments were carried out in duplicate using a 150 rpm orbital shaker. Two (2) g of the materials was put in 250 mL amber bottles containing benzene solution with initial concentrations ranging from 2 to 50 mg benzene L^{-1}. No headspace was left in the bottles to avoid losses via volatilization. After agitation samples were taken and analyzed for benzene. Kinetic experiments were also carried out in duplicate using 2 g of sorbents and benzene-contaminated water (20 mg L^{-1}). Samples were taken at different time intervals (20, 40, 60, 80, 100, and 120 min) and analyzed for benzene. The amount of benzene adsorbed per unit weight of the adsorbent at equilibrium q_e was calculated using Eq. (3), while Eq. (4) was used to determine the amount removed at a particular time.

$$q_e = v\left(\frac{C_0 - C_e}{m}\right) \quad (3)$$

$$q_t = v\left(\frac{C_0 - C_t}{m}\right) \quad (4)$$

where: q_e is the amount of benzene adsorbed (mg g^{-1}) at equilibrium; C_0 and C_e are the initial and equilibrium benzene concentrations in mg L^{-1}, respectively; m is the mass of the adsorbent (g); v is the volume of the solution (L); q_t is the amount sorbed at a time (t) (mg g^{-1}), and C_t is the concentration at time (t) (mg L^{-1}).

The linear forms of the Freundlich and Langmuir adsorption isotherms were applied to the experimental data (Osagie and Owabor, 2015; Mohammadi et al., 2017). The Freundlich model assumes that the adsorbent's surface is heterogeneous and can be used to describe both monolayer (chemisorption) and multilayer (physisorption) adsorption processes (Osagie and Owabor, 2015; Mohammadi et al., 2017). The linear form of the Freundlich model is represented by Eq. (5).

$$\log q_e = log K_F + \frac{1}{n} log C_e \quad (5)$$

where: q_e is the amount of benzene adsorbed (mg g^{-1}) at equilibrium; C_e is the equilibrium concentration (mg g^{-1}); K_F and 1/n are the Freundlich isotherm constants related to the adsorption capacity and adsorption intensity, respectively. K_F and 1/n represent the intercept and slope, respectively, when log q_e is plotted against log C_e.

The Langmuir isotherm is valid for monolayer adsorption, and it assumes that the adsorbent has a finite adsorption capacity. Moreover, all the sites on the adsorbent are assumed to be energetically and sterically independent of the sorbed quantity (Osagie and Owabor, 2015; Mohammadi et al., 2017). Eq. (6) is the linear form of the Langmuir isotherm model used in this study.

$$\frac{C_e}{q_e} = \left(\frac{1}{q_{max} b}\right) + \frac{C_e}{q_{max}} \quad (6)$$

where: b is the Langmuir adsorption constant and q_{max} is the maximum adsorption capacity (mg g^{-1}). The slope and intercept of the straight line C_e/q_e versus C_e were used to calculate q_{max} and b of the Langmuir isotherm. Furthermore, the Langmuir adsorption constant b (L mg^{-1}) was used to determine the separation factor (R_L) (Hall et al., 1966), which is expressed as:

$$R_L = \frac{1}{1 + bC_0} \quad (7)$$

The value of R_L indicates the nature of the adsorption process. $R_L < 1$ suggests favourable adsorption, while $R_L > 1$ indicates unfavourable adsorption.

To obtain additional information about the adsorption processes, the experimental data were further analyzed with kinetic models, including the pseudo-first-order (PFO) (Eq. (8)), pseudo-second-order (PSO) (Eq. (9)) (Ho and McKay, 1998), and the intra-particle diffusion (Eq. (10)) (Weber and Morris, 1963) models.

$$log(q_e - q_t) = log q_e - \frac{k_1}{2.303} t \quad (8)$$

$$\frac{t}{q_t} = \frac{1}{k_2 q_e^2} + \frac{1}{q_e} t \quad (9)$$

$$q_t = k_{id}\sqrt{t} + C \quad (10)$$

where: q_t and q_e are the amount of benzene adsorbed (mg g^{-1}) at time t and equilibrium, respectively. k_1 is the rate constant of the PFO kinetic model (min^{-1}), which is determined from the slope of the line log (q_e-q_t) vs t; k_2 is the PSO rate constant (min^{-1}). $\frac{1}{k_2 q_e^2}$ and $\frac{1}{q_e}$ are the intercept and the slope of the straight line, respectively. $k_2 q_e^2$ is the initial or instantaneous sorption rate (mg g^{-1} min^{-1}) (Ho and McKay, 1998); k_{id} is the intra-particle diffusion rate constant (mg g^{-1} $min^{-1/2}$), which can be obtained from the slope of the straight line q_t versus $t^{1/2}$. C is a constant related to the thickness of the boundary layer (Itodo et al., 2010).

2.3. Column experiment

The column experiments were implemented to study the transport of benzene in the media (both individual and mixtures) under dynamic conditions. The materials were air-dried and packed into the columns in incremental steps based on the materials' dry density and volume of the column (Fig. 1). Uncontaminated water was flushed through the columns to establish a steady-state condition. The porosity of the packed bed was quantified by determining the gravimetric moisture content, and the values were subsequently converted to volumetric based on the bulk density of the packed bed. Hydraulic conductivity (K) was measured using the constant head method (e.g., Head and Keeton, 2008) before and after the experiment. Synthetic water spiked with chloride and benzene was introduced into the columns (in an upward flow direction) by step from a Teflon bag (to minimize volatilization) using a peristaltic pump at a flow rate of 1.67 cm^3 min^{-1} (i.e. ca. 0.074 cm min^{-1} linear velocity). The Cl^- was used to characterize physical transport in the media (i.e., to determine whether the transport is Fickian or there are flow anomalies under the used experimental conditions). Table 2 summarises the properties of the packed columns.

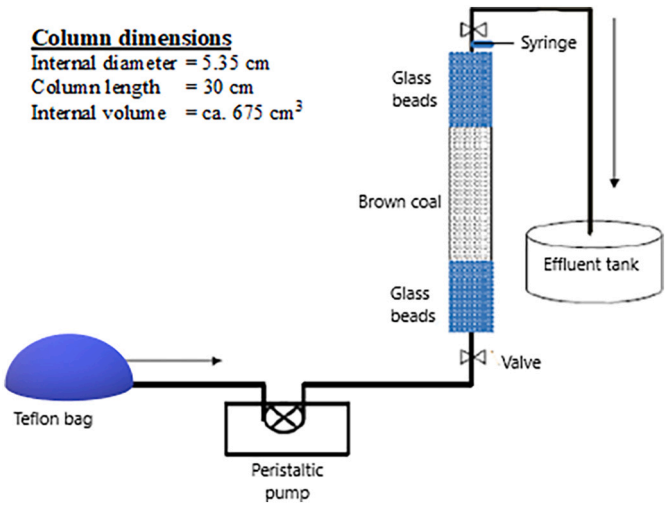

Fig. 1. Setup of the column experiment.

Table 2
Properties of the packed columns.

Material	Mixing ratio	$v_{experiment}$ (cm min^{-1})	ρ_b (g cm^{-3})	n (−)
Brown coal	–	0.19	1.28	0.39
Zeolite	–	0.20	1.28	0.38
Compost	–	0.21	1.24	0.36
Zeolite-compost	1:1	0.19	1.26	0.40
Brown coal-compost	5:1	0.21	1.27	0.35

ρ_b: bulk density of column; $v_{experiment}$: experimentally determined pore water velocity; and n: total porosity.

Effluent samples were taken at specific intervals (i.e. 1, 3, 5, 8, 10, 15, 20, 24, and 30 pore volumes (PVs) for benzene and from 0.1 to 2 PVs for chloride) using a disposable glass syringe fixed to the columns to prevent/minimize benzene loss via volatilization. Observed concentrations, C, were normalized to the initial concentration, C_0, to enable the comparison of the breakthrough curves (BTCs). Time was also normalized to the mean residence time (MRT) to obtain the pore volumes flushed.

2.4. Analytical methods

The liquid-liquid extraction (LLE) method (Glaze and Lin, 1983) was used in this study. Five (5) mL of the effluent sample was transferred into a vial capped with Teflon-lined septa after which 1 mL of n-pentane was added and agitated for 5 min to reach liquid-liquid equilibrium. The pentane extract was then transferred into 2.5 mL glass vials capped with Teflon-lined septa and analyzed for benzene using gas chromatography (Shimadzu GC 17A, PAF/A/5/Sb). Chloride was determined titrimetrically using $AgNO_3$ as the standard and K_2CrO_4 as the indicator (Richards, 1968). For reproducibility of the results, all the experiments were performed in duplicate and average values were used. Additionally, blank experiments were carried out to assess losses via volatilization.

2.5. Modelling approach

The ADE is an equilibrium model that considers advection and dispersion as the fundamental processes governing the fate and transport of solute. Dispersion is assumed to behave macroscopically as a Fickian process with dispersivity remaining constant in space and time. Consequently, the basic form of the ADE is unable to reproduce non-Fickian or anomalous processes due to its inability to account for the effects of pore-scale fluctuations (Köhne et al., 2006). The ADE can, however, be modified to account for other biotic and abiotic processes such as retardation due to reversible sorption, biodegradation, and/or nonequilibrium processes. In the present study, one-dimensional (1-D) analytical solutions of the ADE (Eqs. (11) and (12)) were formulated to describe, respectively, chloride and benzene transport in the studied media (Domenico and Schwartz, 1998; Thornton et al., 2000).

$$\frac{C}{C_0} = \frac{1}{2}\, erfc\left[\frac{z - v_p t}{2(\alpha v_p t)^{1/2}}\right] + \frac{1}{2}\, exp\left(\frac{v_p z}{\alpha v_p}\right) erfc\left[\frac{z + v_p t}{2(\alpha v_p t)^{1/2}}\right] \tag{11}$$

$$\frac{C}{C_0} = \frac{1}{2} exp\left\{\left(\frac{z}{2\alpha}\right)\left[1 - \left(1 + \left(\frac{4\mu\alpha}{v_p}\right)\right)^{\frac{1}{2}}\right]\right\} \times erfc\left[\frac{Rz - v_p t\left(1 + \left(\frac{4\mu\alpha}{v_p}\right)\right)^{\frac{1}{2}}}{2(\alpha v_p t R)^{1/2}}\right] \tag{12}$$

where: C and C_0 are the effluent and input concentrations of the solute (mg L^{-1}); erfc is the complementary error function; v_p is the pore water velocity (cm min^{-1}); R is the retardation factor [−] which is a fully reversible process between the solution and the solid phases; z is the column length or the distance (cm) from the source of contamination after time, t (min); μ (min^{-1}) is a sink that is used to represent irreversible sorption due to physical/sorption-related nonequilibrium processes or biodegradation based on first-order decay (Thornton et al., 2000; Baek et al., 2003; Köhne et al., 2006); α is the dispersivity (cm).

The chloride simulation was performed assuming no retardation ($R = 1$) and decay ($\mu = 0$) of the chloride, and the approach involved reproducing one known parameter (i.e., pore-water velocity) and the other unknown (i.e., dispersivity). These parameters were then fixed in Eq. (12) to simulate the transport of benzene. The μ and R were adjusted until best fits were obtained in the case of benzene. The initial concentration was set to zero for the entire sample, and the boundary conditions were $C = 0$ at an infinite distance from the inlet and $C = C_0$ at the inlet for all the solute transport processes in this study. Additional parameters describing chloride and benzene transport, namely: effective porosity, n_e, hydrodynamic dispersion coefficient, D_L (cm^2 min^{-1}), Péclet number, *Pe*, and experimental partition coefficient (K_d^e), were calculated using Eqs. (13) to (16), respectively. The theoretical distribution coefficient (K_d^t), was also determined using Eq. (17) for comparison with the K_d^e. This relationship normally holds when the f_{oc} is >0.1% (Appelo and Appelo and Postma, 1993; Thornton et al., 2000; Zheng et al., 2002).

$$n_e = \frac{Q}{A \times v_p} \tag{13}$$

$$D_L = \alpha_L \times v_p \tag{14}$$

$$P_e = \frac{v_p \times z}{D_L} \tag{15}$$

$$K_d^e = \frac{(R - 1) \bullet n_e}{\rho_b} \tag{16}$$

$$K_d^t = K_{oc}^t \times f_{oc} \tag{17}$$

where: Q: discharge (cm^3 min^{-1}); A: the cross-sectional area of the column (cm^2); D_L: the hydrodynamic dispersion coefficient (cm^2 min^{-1}) assuming negligible diffusion; α: the dispersivity (cm); ρ_b: the bulk density (g cm^{-3}); *Pe*: Péclet number [−]. *Pe* indicates the relative importance of mechanical dispersion and molecular diffusion in the transport of solute in the media, where $Pe < 0.4$ indicates that the solute transport is controlled mainly by molecular diffusion, *Pe* between 0.4 and 6 indicates the combined effects of molecular diffusion and mechanical dispersion on the solute transport, and $Pe > 6$ indicates the

dominance of mechanical dispersion over molecular diffusion (Fetter, 2001); K_d^e and K_d^t, respectively, represent the experimental and theoretical partition coefficient ($cm^3\ g^{-1}$); f_{oc} represents the fraction of OC in the reactive material; K_{oc}^t is the theoretical solute distribution coefficient to solid OC. The value of K_{oc}^t used in this calculation was taken from Weiner (2008). The accuracy of the simulations was evaluated based on the correlation coefficient (R^2) and root mean square error (RMSE) (Eq. (18)). The smaller (closer to 0) the RMSE, the better the model prediction. Higher values of RMSE indicate a large over-or under-estimation of the experimental data by the model.

$$\mathrm{RMSE} = \sqrt{\frac{\sum_{j=1}^{N}\left[\left(\frac{C}{C_0}\right)_{cal} - \left(\frac{C}{C_0}\right)_{exp}\right]^2}{N}} \tag{18}$$

where: $\left(\frac{C}{C_0}\right)_{cal}$ and $\left(\frac{C}{C_0}\right)_{exp}$, respectively, are the predicted and measured relative concentration at time t; N is the number of observations.

Additional properties including the removal efficiency and removal capacity of the adsorbents were determined using the equations below (Obiri-Nyarko et al., 2020):

$$\mathrm{RE}_{\%} = \left[\left(\frac{Q}{1000}\int_0^{t_{total}} C_{rem}\,dt\right) \Big/ \left(\frac{C_0 Qt_{total}}{1000}\right)\right] \times 100 \tag{19}$$

$$q_{TRC} = \left[\left(\frac{Q}{1000}\int_0^{t_{total}} C_{rem}\,dt\right) \Big/ m\right] \tag{20}$$

where: m (mg) is the mass of the adsorbent in the columns; t_{total} represents the total experimental time (min), Q is the flow rate ($cm^3\ min^{-1}$); $C_{rem} = (C_0 - C_t)$ is the reduction of the benzene concentration in the effluent due to sorption ($mg\ dm^{-3}$); C_0 and C_t ($mg\ dm^{-3}$) are the initial benzene concentration and concentration at time t; $RE_{\%}$, (%) is the rate of benzene removal; q_{TRC} ($mg\ g^{-1}$) is the total removal capacity of the material.

3. Results and discussion

3.1. Batch experiment

3.1.1. Adsorption isotherms and kinetics models

The results of fitting the two isotherms to the experimental data are illustrated in Fig. 2a & b, while the estimated parameter values are summarized in Table 3. A high correlation coefficient ($R^2 \geq 0.96$) was obtained for the two isotherms, indicating that both models can be utilized to characterize benzene adsorption onto the examined sorbents. This suggests the existence of both monolayer and heterogeneous surface conditions on the adsorbents. The R_L values obtained from the Langmuir isotherm ranged from 0.03 to 0.45 for zeolite, 0.01–0.14 for brown coal, and 0.02–0.37 for compost indicating that the adsorption of benzene onto the studied adsorbents is favourable. Similarly, the values of 1/n determined from the Freundlich isotherm were < 1, indicating favourable adsorption (Özer and Pirincci, 2006). Among the studied materials, brown coal demonstrated the highest capacity to remove benzene. The maximum adsorption capacity (q_{max}) determined with the Langmuir model was 6.057 mg g^{-1} for brown coal, which is generally higher when compared to the q_{max} of the natural adsorbents (e.g., clay and sand) but lower when compared to the q_{max} of synthetic or modified/treated adsorbents (Table 4).

The kinetics of contaminant removal is important in PRB studies as it indicates the rate and removal mechanisms, which are crucial for the design of PRBs. The results of the kinetics studies are shown in Fig. 3a-c while the kinetic constants and R^2 are reported in Table 5. Although the values of R^2 for both PFO and PSO kinetic models are high (>0.94), the adsorption capacities calculated by the PSO model are closer to those determined experimentally when compared to those determined with the PFO model. This indicates that the adsorption of benzene onto the

Table 3
Isotherm parameters for adsorption of benzene onto compost, brown coal and zeolite.

Isotherm	Parameter	Brown coal	Zeolite	Compost
Langmuir	b (L mg^{-1})	3.052	0.612	0.837
	q_{max} (mg g^{-1})	6.057	3.484	2.823
	R^2	0.983	0.979	0.960
	R_L	0.01–0.14	0.031–0.45	0.02–0.37
Freundlich	K_F (mg g^{-1})(L $mg^{-1})^{1/n}$	12.368	6.066	7.836
	1/n	0.477	0.367	0.303
	R^2	0.997	0.986	0.995

b: Langmuir constant related to the energy of adsorption or adsorption intensity; q_{max}: maximum adsorption capacity determined from the Langmuir isotherm; K_F: Freundlich constant related to the saturation capacity of the sorbent; 1/n: adsorption intensity; and R^2: correlation coefficient.

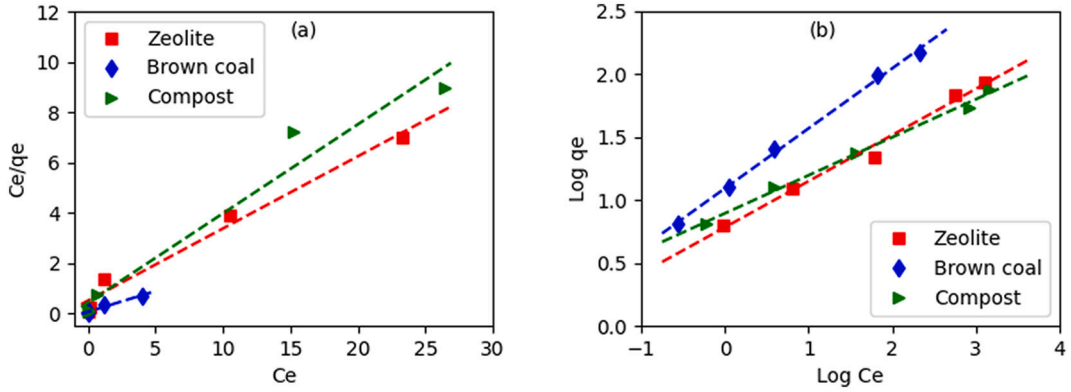

Fig. 2. Linear fittings of the (a) Langmuir and (b) Freundlich isotherm models to the experimental data for zeolite, brown coal, and compost. (For interpretation of the references to colour in this figure legend, the reader is referred to the web version of this article.)

Table 4
Comparison of benzene adsorption capacities of adsorbents in this study with other.

Adsorbent	q_{max} (mg g^{-1})	References
PMO	7.04	Moura et al. (2011)
CKD	130.39	Faisal et al. (2021)
PEG-Mt	5.92	Nourmoradi et al. (2012)
SMZ	150.42	Vidal et al. (2012)
F-400	183.29	Wibowo et al. (2007)
F-400Cox	114.41	Wibowo et al. (2007)
F-400Tox	240.07	Wibowo et al. (2007)
CuO-NPs	100.24	Mohammadi et al. (2017)
Natural clay	1.26	Osagie and Owabor (2015)
Sandy soil	1.14	Osagie and Owabor (2015)
Brown coal	6.06	Present study
Zeolite	3.48	Present study
Compost	2.82	Present study

PMO: periodic mesoporous organosilicas; CKD: cement kiln dust; PEG—Mt: montmorillonite (Mt) modified with poly ethylene glycol; SMZ: HDTMA-modified Y zeolite; (F-400): granular activated carbon Filtrasorb400; F-400Cox: chemically treated granular activated carbon Filtrasorb400; F-400Tox: thermally treated granular activated carbon Filtrasorb400; and CuO-NPs: copper oxide nanoparticles.

studied materials is a chemical process (chemisorption) involving sharing of electrons between benzene and the surface of the sorbents. Similar results were reported by Simantiraki and Gidarakos (2015). The intra-particle diffusion model (Weber and Morris, 1963) was employed to explore the effect of diffusion on the mass transfer of benzene onto the studied materials. According to Tan and Hameed (2017), solute mass transfer occurs in three steps: (i) film diffusion (external diffusion); (ii) pore diffusion (i.e. intra-particle diffusion); and (iii) surface reaction, which involves the attachment of the adsorbate to the internal surface of the adsorbent. According to Weber and Morris (1963), the plot of qt vs $t^{1/2}$ will produce a straight line with a slope K_{id}, which represents the intra-particle diffusion rate constant, and an intercept, C, which indicates the thickness of the boundary layer or surface adsorption. If the straight line passes through the origin, it indicates that intra-particle diffusion is the only mechanism and the rate-limiting step in the adsorption process. It can be seen from Fig. 3c that the linear plots did not pass through the origin, indicating that intra-particle diffusion is not the rate-limiting step and the only mechanism controlling the adsorption process.

Table 5
Kinetic parameters for adsorption of benzene onto brown coal, compost, and zeolite.

Model	Parameter	Brown coal	Zeolite	Compost
Pseudo-1st-order (PFO)	$qe_{(exp)}$ (mg g^{-1})	2.509	2.212	2.291
	$qe_{(cal)}$ (mg g^{-1})	2.221	1.112	1.039
	k_1(min^{-1})	0.020	0.006	0.006
	R^2	0.946	0.963	0.997
Pseudo-2nd-order (PSO)	k_2(g mg^{-1} min^{-1})	0.015	0.015	0.017
	$q_{e(exp)}$ (mg g^{-1})	2.509	2.212	2.291
	k_2q^2 (mg g^{-1} min^{-1})	0.112	0.078	0.095
	q_e(cal) (mg g^{-1})	2.750	2.260	2.352
	R^2	1.000	0.994	0.999
Intra-particle diffusion	K_{id} (mg g^{-1} $min^{-1/2}$)	0.083	0.066	0.067
	C	1.291	1.032	1.151
	R^2	0.923	0.984	0.980

$qe_{(cal)}$: theoretical adsorption capacity; $qe_{(exp)}$: experimental adsorption capacity; k_1: PFO adsorption rate constant; R^2: correlation coefficient; k_2: PSO rate constant; k_2q^2: initial or instantaneous sorption rate; K_{id}: intra-particle diffusion rate constant; and C: intra-particle diffusion boundary layer thickness.

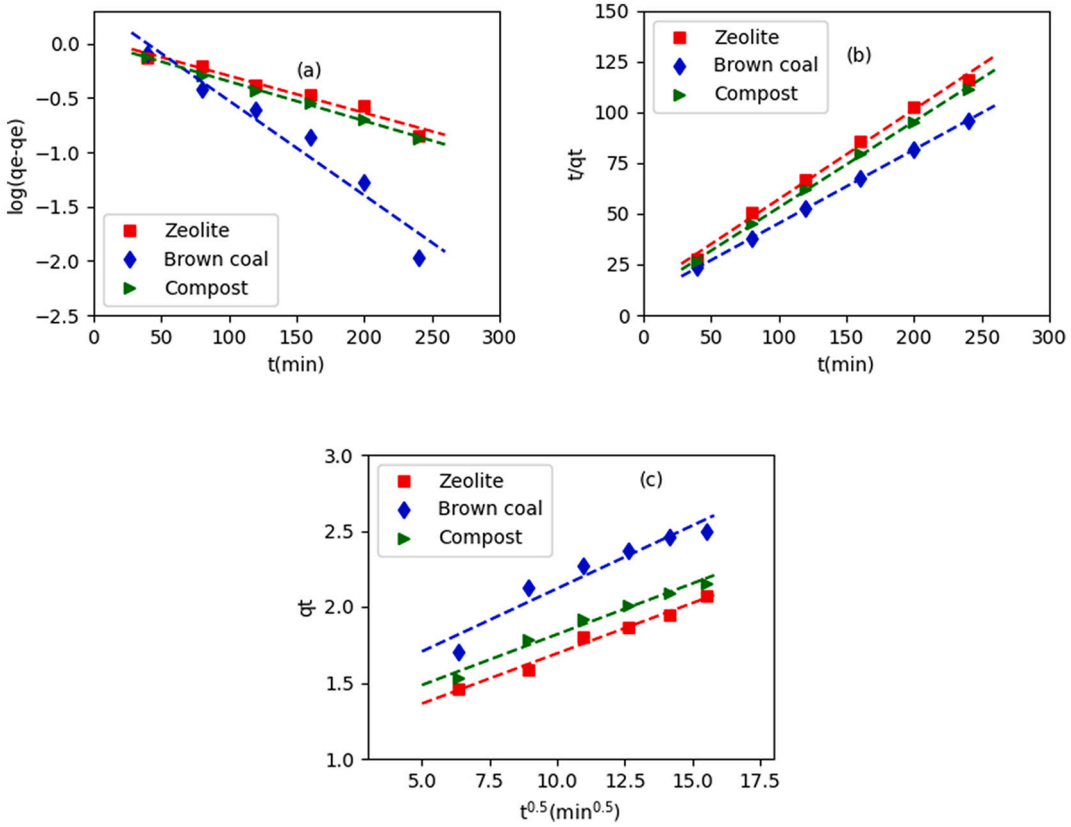

Fig. 3. Fittings of the experimental kinetic data with the (a) PFO; (b) PSO; and (c) Intra-particle diffusion models.

3.2. Column studies

3.2.1. Chloride breakthrough curves

Physical or transport-related nonequilibrium, also known as anomalous (non-Fickian or nonideal) transport (e.g., preferential flow), is a major issue in PRBs as it limits the mass transfer of contaminants to the reactive sites, resulting in lower than expected barrier performance (Kamolpornwijit et al., 2003). The chloride experiments were conducted to ascertain the presence of physical or transport-related nonequilibrium in the columns based on the experimental data and curve fitting with the ADE. Several researchers (e.g., Singh and Kanwar, 1991; Köhne et al., 2006) have noted that physical or transport-related nonequilibrium (e.g., preferential flow and diffusion into non-advective zones) exists if the ADE is unable to adequately describe the non-reactive tracer transport, or if 50% of the injected chloride ($C/C_0 = 0.5$) is measured in the effluent well before or after 1 PV.

Fig. 4a-e shows the experimental and simulated Cl^- BTCs for the different media. Since samples were collected at the outlet of each column, the measured BTCs reflect the macroscopic behaviour of the column. As can be seen, the Cl^- BTCs have different shapes, reflecting different transport conditions in the media. The values of the inverted

Table 6
The hydrodynamic parameters estimated from the chloride curve fitting.

Reactive materials	v_p (cm min^{-1})	D_L (cm^2 min^{-1})	α (cm)	*Pe* (−)	n_e (−)	R^2	RMSE
Brown coal	0.20	0.42	2.10	14.2	0.37	0.985	0.050
Zeolite	0.23	1.15	5.00	6.0	0.32	0.983	0.049
Compost	0.21	0.43	2.10	14.7	0.36	0.980	0.058
Zeolite-compost	0.19	0.61	3.17	9.3	0.39	0.986	0.048
Brown coal-compost	0.22	0.24	1.10	27.5	0.32	0.990	0.042

D_L: hydrodynamic dispersion coefficient; α: dispersivity; v_p: pore-water velocity; *Pe*: Péclet number; n_e: effective porosity; RMSE: root mean square error; and R^2: correlation coefficient.

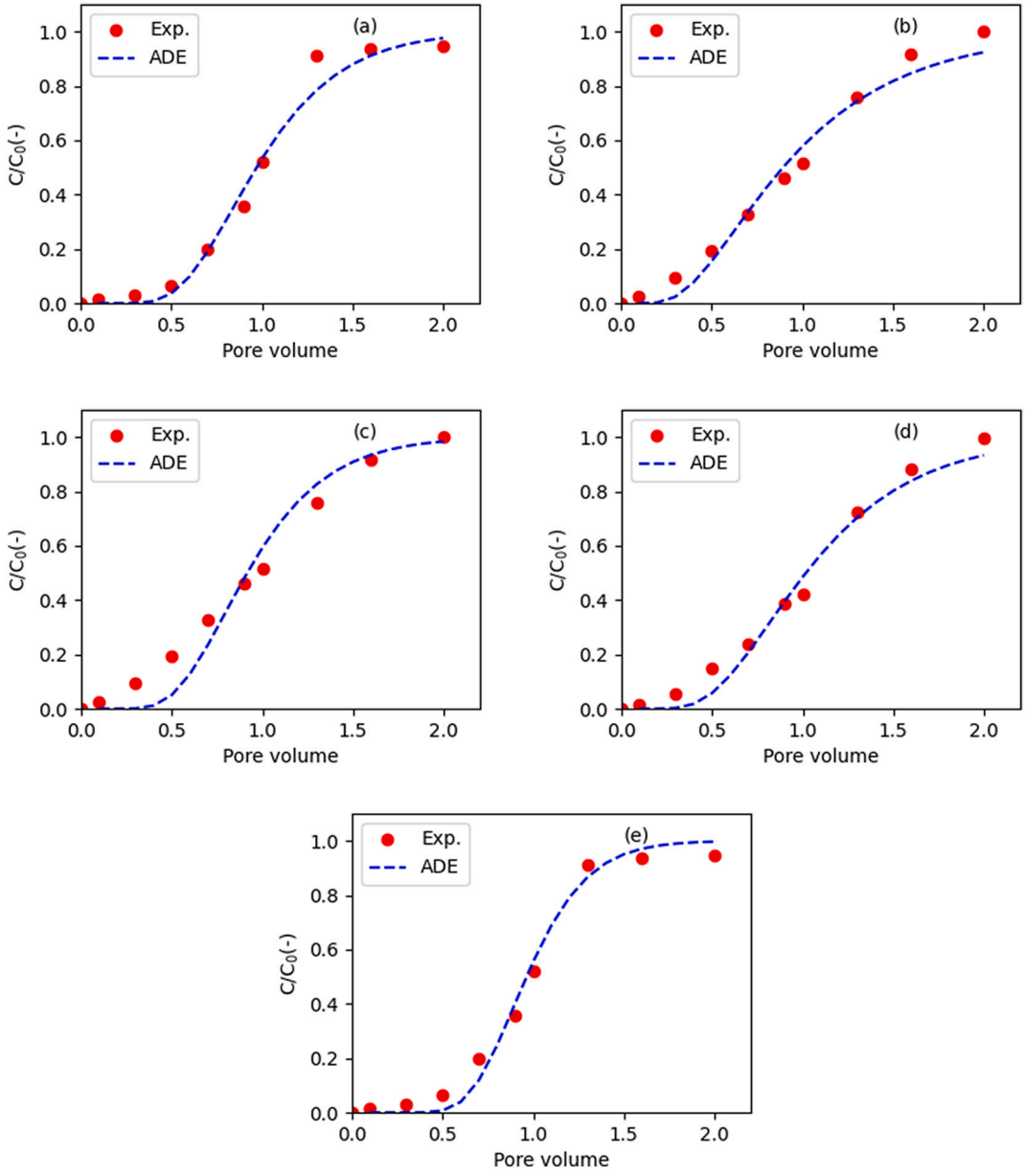

Fig. 4. Experimental and modelled BTCs of chloride in (a) brown coal, (b) zeolite, (c) compost, (d) zeolite-compost, and (e) brown coal-compost. (For interpretation of the references to colour in this figure legend, the reader is referred to the web version of this article.)

parameters (i.e. pore-water velocity and dispersivity) are summarized in Table 6. The model results for pore-water velocity compared well with the calculated pore-water velocity obtained from the ratio of flux rate to water content (Table 2). Effective porosity was slightly lower than the total porosity in all the columns except the column with compost, indicating negligible immobile water zones in the columns. Dispersivity ranged from 2.1 to 5.0 cm, with lower values indicating lower variability in the microscopic velocity distribution (e.g., Kumahor et al., 2015) and reduced spread in solute breakthrough. The corresponding Péclet numbers for the columns ranged from 6 to 27.5, indicating that the flow regime within the studied columns was dominated by mechanical dispersion and diffusion into the non-advective or immobile zones was not significant. As shown in Fig. 4a-e, $C/C_0 = 0.5$ was measured a little before or after 1 PV. Moreover, the ADE described all the Cl^- BTCs reasonably well ($R^2 \geq 0.98$ and RMSE <0.06), suggesting that physical or transport-related nonequilibrium processes, such as preferential flow and diffusive transport into immobile zones at the beginning of the experiments were marginal. It should be mentioned that the chloride measurements were terminated after 2 PVs due to analytical difficulties. Therefore, these observations reflect the transport conditions in the media at the beginning and not for the entire duration of the experiment.

3.2.2. *Benzene breakthrough curves*

BTCs showing the behaviour of benzene in the studied media are displayed in Fig. 5a–e**.** In relation to the chloride BTCs (Fig. 4a-e), the benzene BTCs shifted to the right on the time axis (PV), indicating benzene retardation by the media. The effluent concentration of benzene from all the columns was also below the inlet concentration ($C/C_0 < 1$) except for zeolite where there was 100% recovery of the applied benzene, i.e. $C/C_0 = 1$. The benzene BTC of the brown coal column additionally showed a plateau between PV 10 and 15 after which benzene concentration started to decline again. Volatilization, biodegradation, and nonequilibrium processes (e.g., sorption- and transport-related nonequilibrium) have been adduced as possible causes of such behaviour (Selim et al., 1999; Thornton et al., 2000; Baek et al., 2003; Köhne et al., 2006; Parashar et al., 2007). In the present study, however,

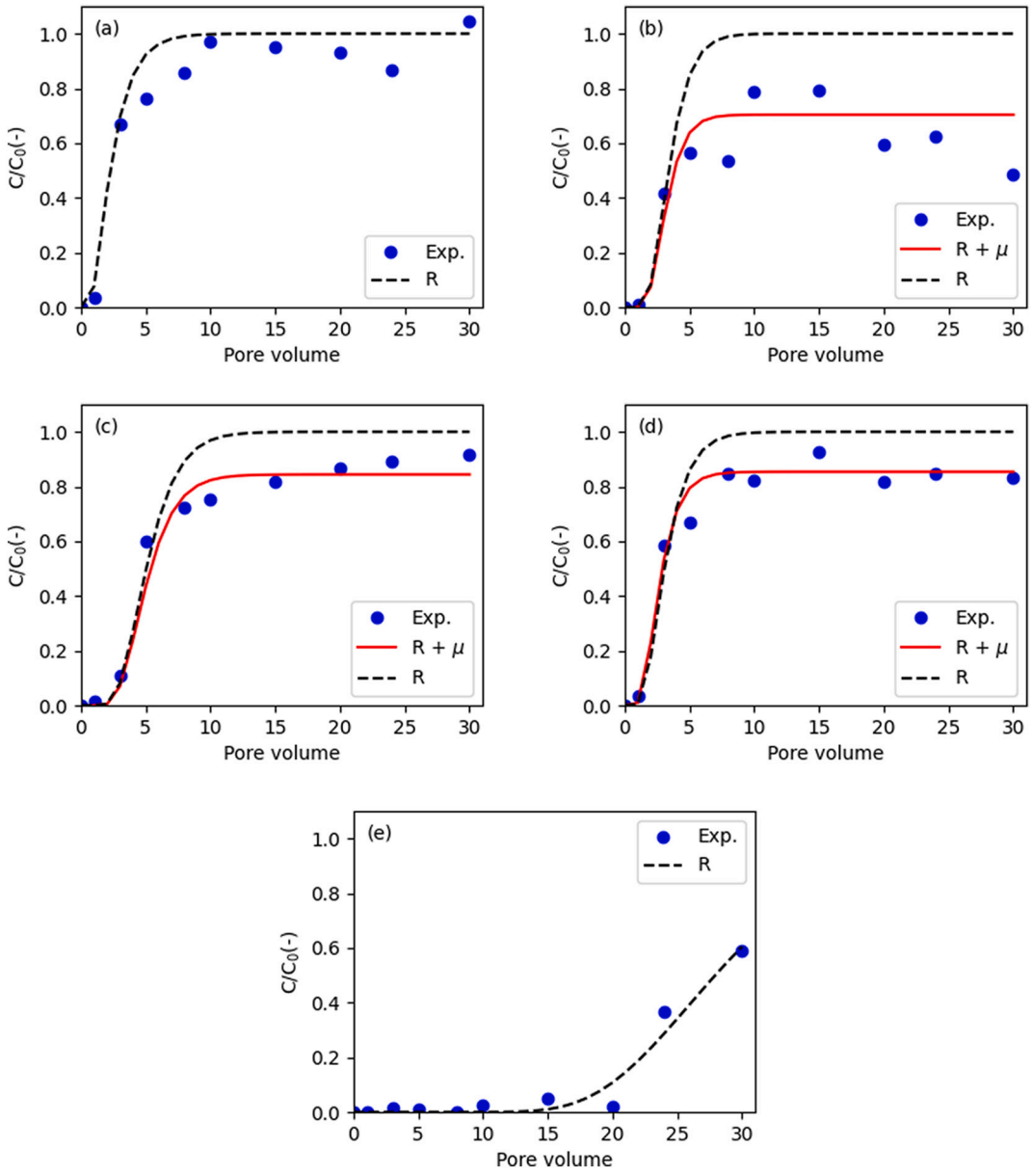

Fig. 5. Modelled and experimental BTCs of benzene in: (a) zeolite, (b) brown coal, (c) compost, (d) zeolite-compost, and (e) brown coal-compost columns. (For interpretation of the references to colour in this figure legend, the reader is referred to the web version of this article.)

we attribute the observed $C/C_0 < 1$ as well as the plateau to physical/sorption nonequilibrium processes with biodegradation playing little or no role. Volatilization is ruled out since benzene mass loss in the blank experiments (without sorbents) was insignificant.

In a related study by Grajales-Mesa and Malina (2019), the authors observed that the application of compost resulted in the biodegradation of trichloroethylene. In the present study, biodegradation has been considered a benzene mass loss mechanism only because of the nature of the benzene BTCs. We initially did not consider that benzene biodegradation would advance significantly in the columns with compost due to the short duration (70 h) of the experiment. The nonequilibrium processes are classified into physical/transport- and sorption-related nonequilibrium. Sorption-related nonequilibrium can be caused by chemical nonequilibrium (i.e. rate-limited interactions between the sorbate and sorbent) and/or rate-limited diffusive mass transfer (film diffusion, retarded intraparticle diffusion, and intra-sorbent diffusion) while physical nonequilibrium may occur when there is preferential flow and solute diffusion into non-advective/immobile regions of the medium (Brusseau et al., 1991). Köhne et al. (2006) noted that both nonequilibrium processes can cause $C/C_0 < 1$. In the present study, the nonequilibrium processes playing a major role are the intra-organic matter diffusion and benzene transport in preferential flow paths. Diffusive mass transfer into non-advective zones is not favoured since results from the tracer experiment indicated the dominance of mechanical dispersion over molecular diffusion. Brusseau et al. (1991) also noted that the specific sorbate-sorbent interaction is relatively irrelevant for hydrophobic organic compounds (HOCs) since their sorption is generally driven by partitioning between the solution and OM components of the sorbent. On the contrary, they found intra-sorbent (intra-organic matter) mass transfer diffusion as the main cause of the sorption nonequilibrium of HOC due to the polymeric nature of OM. Sander and Pignatello (2009) reported that intra-sorbent diffusion is mostly an irreversible process, resulting in effluent concentrations generally lower than the influent solute concentrations. The preferential flow, on the other hand, causes contaminants to bypass reactive sites, resulting in higher effluent solute concentration (Kamolpornwijit et al., 2003). It is possible that in addition to intra-sorbent (intra-organic matter) mass transfer diffusion, preferential flow also occurred in the columns. The ascending part of the plateau observed in the brown coal column, for example, is reminiscent of preferential flow. It is worth noting that, as the experiments proceeded, particles from columns with brown coal and compost were detected in the effluent, indicating attrition and possible rearrangement in those media. This structural rearrangement possibly created preferential flow paths in those columns, allowing contaminants to bypass the reactive sites.

The capability of the used model to predict benzene transport in the studied media and to estimate the benzene attenuation parameters was also explored. The results are shown in Fig. 5a-e. The ADE where only R was considered could only reproduce sufficiently the experimental data for zeolite and the brown coal-compost mixture, indicating that benzene removal by these sorbents is a reversible process. In the case of the brown coal-compost mixture, the BTC was incomplete, so it is unclear whether other processes apart from reversible sorption were involved. For the other systems (brown coal, compost, zeolite-compost mixture), significant disparities between the experimental and modelled results were observed. However, when both R and μ were coupled and fitted to the experimental data, significant improvement in the simulation was observed.

The estimated values of R and μ are summarized in Table 7. Benzene was most retarded by the brown coal-compost mixture ($R = 29$) while zeolite exhibited the least affinity for benzene ($R = 2.8$). This is possibly due to the relatively high f_{oc} of the brown coal-compost mixture and the relatively small grain size of the brown coal (Table 1) (Müller, 2010). The corresponding experimental distribution coefficient, K_d^e ranged from 0.45 to 7.11 $cm^3\ g^{-1}$. The K_d^t calculated for each column material based on literature data of K_{oc} and OC contents of the media is also shown in Table 7. The K_d^t indicates the expected sorption in a model system where other influencing processes are limited. The use of Eq. (17) to calculate the distribution coefficient is justified since the OC values measured for all the studied materials except zeolite were > 0.1% ($f_{oc} > 0.001$). This represents a condition where hydrophobic partitioning onto OC is equal to non-hydrophobic sorption by minerals (Thornton et al., 2000). The calculated K_d^t values ranged from 1.78 to 11.92 $cm^3\ g^{-1}$, which are 1.5 to 11.8 times higher than the K_d^e values, implying that the performance of the materials was lower than expected. This could be due to benzene transport in preferential pathways as explained earlier and/or the high pore-water velocity used, which is inversely related to R (e.g., Pang et al., 2002; Kim et al., 2006a). Pang et al. (2002) explained that at low flow rates, there is a longer retention of the contaminants in the columns, which allows for more complete sorption. The R factors and some experimental conditions reported in other studies are summarized in Table 8 for comparison with the values from the present study. As can be seen, the R obtained for the brown coal-compost mixture is generally higher than those for the other reported media.

Table 7
Estimated parameters from the benzene BTCs.

Material	R	K_d^e ($cm^3\ g^{-1}$)	K_d^t ($cm^3\ g^{-1}$)	μ (min^{-1})	RE (%)	q_{TRC} ($mg\ g^{-1}$)
Brow coal	4	0.87	10.20	8.0×10^{-4}	51.87	8.05×10^{-2}
Zeolite	2.8	0.45	1.78	0.0	11.11	1.95×10^{-2}
Compost	6	1.45	11.92	2.0×10^{-4}	33.33	9.62×10^{-2}
Zeolite-compost	2.9	0.58	6.85	3.5×10^{-4}	22.08	4.63×10^{-2}
Brown coal-compost	29	7.11	10.49	0.0	90.12	16.15×10^{-2}

R: retardation factor; K_d^e: experimental partition coefficient; K_d^t: theoretical distribution coefficient; μ: degradation rate; q_{TRC}: total removal capacity; and RE: removal efficiency.

The values of μ ranged from 0 to $8 \times 10^{-4}\ min^{-1}$. For zeolite and the brown coal-compost mixture, $\mu = 0$ was obtained, indicating that benzene removal was due to its retardation or reversible sorption. For the other columns, benzene removal was possibly due to reversible sorption and biodegradation, and/or irreversible sorption due to the diffusive mass transfer of benzene into the matrix of OM. The effect of biodegradation could have been quantified by performing sterile (involving the application of a biocidal compound to annihilate microorganisms) and non-sterile tests (Kiecak et al., 2020). However, as indicated earlier, we did not anticipate that biodegradation would occur within the experimental period, so such experiments were not performed. Advanced models together with additional experiments (e.g., two-site and two-region models and sterile and non-sterile experiments) to distinguish between these processes will be needed (Pang et al., 2002; Kiecak et al., 2020). Additional parameters determined to evaluate the performance of the materials such as their removal efficiency and removal capacity are also presented in Table 7. The removal efficiencies ranged from 11.11 to 90.12% while the removal capacity ranged from 1.95×10^{-2} to $16.15 \times 10^{-2}\ mg\ g^{-1}$. The highest removal efficiency and adsorption capacity were obtained for the brown coal-compost mixture. This implies that a smaller amount of this mixture will be needed to treat a given volume of benzene-contaminated groundwater as compared to the other adsorbents.

3.3. Hydraulic performance

Evaluating the hydraulic performance of potential PRB materials for in situ groundwater remediation is crucial because many of the reported PRBs failures were caused by changes (increase/decrease) in porosity and hydraulic conductivity of the medium (e.g., Henderson and Demond, 2007). Table 9 displays the hydraulic conductivity values

Table 8
Comparison of sorption parameters reported in the literature and this study.

Reactive material	K_d ($cm^3\ g^{-1}$)	R (−)	Initial concentration (mg dm^{-3})	Flow velocity (cm s^{-1})	Reference
SAM	–	1.02	5.20	0.025	[1]
Triassic sandstone	0.14	1.56	0.39	5.21×10^{-5}	[2]
SAM + PAC	–	1.5–3.2	300	1.69×10^{-3}	[3]
Aquifer material	–	14.3	0.52–1.25	5.2×10^{-4}	[4]
SAM	–	2.46	30	9.72×10^{-3}	[5]
SMZ	–	18.22	9.37	0.027	[6]
SMZ	13.1	–	1.37	0.042	[7]
Brow coal	0.87	4	2.40	1.24×10^{-3}	Present study
Zeolite	0.45	2.8	2.40	1.24×10^{-3}	Present study
Compost	1.45	6	2.40	1.24×10^{-3}	Present study
Zeolite-compost	0.58	2.9	2.40	1.24×10^{-3}	Present study
Brown coal-compost	7.11	28.9	2.40	1.24×10^{-3}	Present study

SAM: sandy aquifer material; SMZ: surfactant-modified zeolite; K_d: partition coefficient; R: retardation factor; PAC: powdered activated carbon. The amount of PAC added ranged from 0 to 2%. [1] Thierrin et al., 1995; [2] Thornton et al., 2000; [3] Kim et al., 2006b; [4] Priddle and Jackson, 1991 [5] Maraqa et al., 1998; [6] Simpson and Bowman, 2009; and [7] Altare et al., 2007.

Table 9
Initial and final hydraulic conductivities of the studied media.

Reactive material	Initial	Final
Brow coal	4.20×10^{-5}	4.30×10^{-5}
Zeolite	2.14×10^{-3}	1.71×10^{-3}
Compost	1.12×10^{-3}	1.03×10^{-3}
Zeolite-compost	1.42×10^{-3}	1.71×10^{-3}
Brown coal-compost	5.77×10^{-5}	6.67×10^{-5}

measured before and after solute injection into the columns. The initial K ranged from 4.20×10^{-5} to 2.14×10^{-3} cm s^{-1}, with the observed discrepancy due to differences in the grain size of the materials. The initial K of the mixtures either increased or decreased relative to their individual components due to similar reasons as adduced above. Although the final K remained within the same order of magnitude after about 70 h of operation, slight changes (increase/decrease) were observed. This is attributed to either particle attrition due to the employed flow rate or reorganization of the pore space by the flowing water as some of the material grains were observed in the effluent from the columns containing compost and brown coal. In general, all the studied media can conduct water fairly well. As a general rule, however, the initial K of the PRB must be greater than that of the aquifer material, and changes in K during the operation of the barrier must not be extreme as this will result in insufficient contact between the contaminant and the reactive material.

4. Conclusion

Laboratory (batch and column) experiments coupled with analytical modelling enabled us to evaluate reactive materials of a PAB for sustainable removal of benzene from contaminated groundwater. The results showed that the brown coal-compost mixture can be used as a low-cost effective reactive material in PABs for remediating benzene-contaminated groundwater. It proved to be the most suitable option among the studied media as it exhibited relatively high (i) ability to retard benzene migration ($R = 29$), (ii) removal efficiency (>90%), and (iii) total removal capacity (0.16 mg g^{-1}), owing to its relatively high OM content and small gain size. Moreover, it can conduct water fairly well ($K = 10^{-3}$ m s^{-1}). Benzene generally exhibited a non-Fickian/nonideal behaviour in all the studied media, which is attributed to sorption- and transport-related nonequilibrium processes (preferential flow and intra-organic matter mass transfer diffusion), and possibly biodegradation. The 1-D ADE modified to include retardation with or without degradation/irreversible sorption allowed satisfactory fit of the model to the experimental benzene BTCs. Further modelling and experimental studies are, however, needed to differentiate between the benzene removal processes. Such discrimination is indispensable for a mechanistic understanding of the dynamics of benzene removal by the sorbents as well as for the design of an effective PAB system for the remediation of benzene-contaminated groundwater.

CRediT authorship contribution statement

Franklin Obiri-Nyarko: Conceptualization, Methodology, Formal analysis, Investigation, Writing - original draft, Writing - review & editing. **Jolanta Kwiatkowska-Malina:** Conceptualization, Methodology, Validation, Formal analysis, Resources, Writing – review & editing. **Samuel Kwame Kumahor:** Software, Formal analysis, Writing - review & editing. **Grzegorz Malina:** Conceptualization, Methodology, Validation, Formal analysis, Resources, Writing – review & editing.

Declaration of Competing Interest

The authors declare no conflict of interest in relation to this work.

Acknowledgement

The research leading to these results has received funding from the European Community's Seventh Framework Programme (FP7/2007-2013 under grant agreement n° 265063).

References

Al-Shammary, A.A.G., Kouzani, A.Z., Kaynak, A., Khoo, S.Y., Norton, M., Gates, W., 2018. Soil bulk density estimation methods: a review. Pedosphere 28, 581–596. https://doi.org/10.1016/S1002-0160(18)60034-7.

Altare, C.R., Bowman, R.S., Katz, L.E., Kinney, K.A., Sullivan, E.J., 2007. Regeneration and long-term stability of surfactant-modified zeolite for removal of volatile organic compounds from produced water. Microporous Mesoporous Mater. 105, 305–316. https://doi.org/10.1016/j.micromeso.2007.04.001.

Appelo, C.A.J., Postma, D., 1993. Geochemistry, Groundwater and Pollution. AA Balkema, Rotterdam.

Baek, D.S., Kim, S.B., Kim, D.J., 2003. Irreversible sorption of benzene in sandy aquifer materials. Hydrol. Process. 17, 1239–1251. https://doi.org/10.1002/hyp.1181.

Bahadar, H., Mostafalou, S., Abdollahi, M., 2014. Current understandings and perspectives on non-cancer health effects of benzene: a global concern. Toxicol. Appl. Pharmacol. 276, 83–94. https://doi.org/10.1016/j.taap.2014.02.012.

Bilardi, S., Ielo, D., Moraci, N., Calabrò, P.S., 2016. Reactive and hydraulic behavior of permeable reactive barriers constituted by Fe0 and granular mixtures of Fe0/pumice. Procedia Eng. 158, 446–451. https://doi.org/10.1016/j.proeng.2016.08.470.

Brusseau, M.L., Jessup, R.E., Rao, P.S.C., 1991. Nonequilibrium sorption of organic chemicals: elucidation of rate-limiting processes. Environ. Sci. Technol. 25, 134–142. https://doi.org/10.1021/es00013a015.

Chen, L., Liu, F., Liu, Y., Dong, H., Colberg, P.J., 2011. Benzene and toluene biodegradation down gradient of a zero-valent iron permeable reactive barrier. J. Hazard. Mater. 188, 110–115. https://doi.org/10.1016/j.jhazmat.2011.01.076.

Domenico, P.A., Schwartz, F.W., 1998. Physical and Chemical Hydrogeology. Wiley, New York.

Erto, A., Andreozzi, R., Lancia, A., Musmarra, D., 2010. Factors affecting the adsorption of trichloroethylene onto activated carbons. Appl. Surf. Sci. 256, 5237–5242. https://doi.org/10.1016/j.apsusc.2009.12.110.

Erto, A., Lancia, A., Bortone, I., Di Nardo, A., Di Natale, M., Musmarra, D., 2011. A procedure to design a permeable adsorptive barrier (PAB) for contaminated groundwater remediation. J. Environ. Manag. 92, 23–30. https://doi.org/10.1016/j.jenvman.2010.07.044.

Eykholt, G.R., Elder, C.R., Benson, C.H., 1999. Effects of aquifer heterogeneity and reaction mechanism uncertainty on a reactive barrier. J. Hazard. Mater. 68, 78–101. https://doi.org/10.1016/s0304-3894(99)00032-1.

Faisal, A.A., Jasim, H.K., Naji, L.A., Naushad, M., Ahamad, T., 2021. Cement kiln dust-sand permeable reactive barrier for remediation of groundwater contaminated with dissolved benzene. Sep. Sci. Technol. 56, 870–883. https://doi.org/10.1080/01496395.2020.1746341.

Fetter, C.W., 2001. Contaminant Hydrogeology, 4th ed. Prentice-Hall, Inc., New Jersey.

Freidman, B.L., Terry, D., Wilkins, D., Spedding, T., Gras, S.L., Snape, I., Mumford, K.A., 2017. Permeable bio-reactive barriers to address petroleum hydrocarbon contamination at subantarctic Macquarie Island. Chemosphere 174, 408–420. https://doi.org/10.1016/j.chemosphere.2017.01.127.

Glaze, W.C., Lin, C.C., 1983. Optimization of Liquid-Liquid Extraction Methods for Analysis of Organics in Water. US Environmental Protection Agency, Environmental Monitoring and Support Laboratory.

Grajales-Mesa, S.J., Malina, G., 2019. Pilot-scale evaluation of a permeable reactive barrier with compost and brown coal to treat groundwater contaminated with trichloroethylene. Water 11, 1922. https://doi.org/10.3390/w11091922.

Grajales-Mesa, S.J., Malina, G., Kret, E., Szklarczyk, T., 2020. Designing a permeable reactive barrier to treat TCE contaminated groundwater: numerical modelling/Diseño de una barrera permeable reactiva para el tratamiento de aguas subterráneas contaminadas con tricloroetileno: modelo numérico. Tecnol. Cienc. Agua 11, 78–106. https://doi.org/10.24850/j-tyca-2020-03-03.

Hall, K.R., Eagleton, L.C., Acrvos, A., Vermeulen, T., 1966. Pore- and solid- diffusion kinetics in fixed-bed adsorption under constant pattern conditions. Ind. Eng. Chem. Fundam. 5, 212–223. https://doi.org/10.1021/i160018a011.

Head, K.H., Keeton, G.P., 2008. Permeability, shear strength & compressibility tests. In: Manual of Soil Laboratory Testing, 2. Whittles Publishing, UK.

Henderson, A.D., Demond, A.H., 2007. Long-term performance of zero-valent iron permeable reactive barriers: a critical review. Environ. Eng. Sci. 24, 401–423. https://doi.org/10.1089/ees.2006.0071.

Ho, Y.S., McKay, G., 1998. Kinetic models for the sorption of dye from aqueous solution by wood. Process. Saf. Environ. Prot. 76, 183–191. https://doi.org/10.1205/095758298529326.

Itodo, A.U., Abdulrahman, F.W., Hassan, L.G., Maigandi, S.A., Itodo, H.U., 2010. Intraparticle diffusion and intraparticulate diffusivities of herbicide on derived activated carbon. Researcher 2, 74–86.

Kamolpornwijit, W., Liang, L., West, O.R., Moline, G.R., Sullivan, A.B., 2003. Preferential flow path development and its influence on long-term PRB performance: column study. J. Contam. Hydrol. 66, 161–178. https://doi.org/10.1016/S0169-7722(03)00031-7.

Kiecak, A., Breuer, F., Stumpp, C., 2020. Column experiments on sorption coefficients and biodegradation rates of selected Pharmaceuticals in three aquifer sediments. Water 12, 14. https://doi.org/10.3390/w12010014.

Kim, S.B., Ha, H.C., Choi, N.C., Kim, D.J., 2006a. Influence of flow rate and organic carbon content on benzene transport in a sandy soil. Hydrol. Process.: Int. J. 20, 4307–4316. https://doi.org/10.1002/hyp.6164.

Kim, S.B., Kim, D.J., Yun, S.T., 2006b. Attenuation of aqueous benzene in soils under saturated flow conditions. Environ. Technol. 27, 33–40. https://doi.org/10.1080/09593332708618614.

Köhne, S., Lennartz, B., Köhne, J.M., Šimůnek, J., 2006. Bromide transport at a tile-drained field site: experiment, and one-and two-dimensional equilibrium and non-equilibrium numerical modelling. J. Hydrol. 321, 390–408. https://doi.org/10.1016/j.jhydrol.2005.08.010.

Kumahor, S.K., de Rooij, G.H., Schlüter, S., Vogel, H.-J., 2015. Water Flow and Solute Transport in Unsaturated Sand—A Comprehensive Experimental Approach. https://doi.org/10.2136/vzj2014.08.0105.

Liang, C., Chen, Y.J., 2010. Evaluation of activated carbon for remediating benzene contamination: adsorption and oxidative regeneration. J. Hazard. Mater. 182, 544–551. https://doi.org/10.1016/j.jhazmat.2010.06.066.

Liu, J.H., Maity, J.P., Jean, J.S., Chen, C.Y., Chen, C.C., Ho, S.Y., 2010. Biodegradation of benzene by pure and mixed cultures of Bacillus spp. World J. Microbiol. Biotechnol. 26, 1557–1567. https://doi.org/10.1007/s11274-010-0331-9.

Mahdipanah, H., Tashakori, A., Emamgholizadeh, S., Maroufpoor, E., 2022. An experimental study on the determination of dispersion coefficient in layered soils. Water Supply 22, 2377–2394. https://doi.org/10.2166/ws.2021.359.

Maraqa, M.A., Zhao, X., Wallace, R.B., Voice, T.C., 1998. Retardation coefficients of nonionic organic compounds determined by batch and column techniques. Soil Sci. Soc. Am. J. 62, 142–152. https://doi.org/10.2136/sssaj1998.03615995006200010019x.

Mohammadi, L., Bazrafshan, E., Noroozifar, M., Ansari-Moghaddam, A., Barahuie, F., Balarak, D., 2017. Adsorptive removal of benzene and toluene from aqueous environments by cupric oxide nanoparticles: kinetics and isotherm studies. J. Chemother. https://doi.org/10.1155/2017/2069519.

Moura, C.P., Vidal, C.B., Barros, A.L., Costa, L.S., Vasconcellos, L.C., Dias, F.S., Nascimento, R.F., 2011. Adsorption of BTX (benzene, toluene, o-xylene, and p-xylene) from aqueous solutions by modified periodic mesoporous organosilica. J. Colloid Interface Sci. 363 (2), 626–634. https://doi.org/10.1016/j.jcis.2011.07.054.

Müller, B.R., 2010. Effect of particle size and surface area on the adsorption of albumin-bonded bilirubin on activated carbon. Carbon 48, 3607–3615. https://doi.org/10.1016/j.carbon.2010.06.011.

Nourmoradi, H., Nikaeen, M., Khiadani, M., 2012. Removal of benzene, toluene, ethylbenzene and xylene (BTEX) from aqueous solutions by montmorillonite modified with nonionic surfactant: equilibrium, kinetic and thermodynamic study. Chem. Eng. J. 191, 341–348. https://doi.org/10.1016/j.cej.2012.03.029.

Obiri-Nyarko, F., Grajales-Mesa, S.J., Malina, G., 2014. An overview of permeable reactive barriers for in situ sustainable groundwater remediation. Chemosphere 111, 243–259. https://doi.org/10.1016/j.chemosphere.2014.03.112.

Obiri-Nyarko, F., Kwiatkowska-Malina, J., Malina, G., Kasela, T., 2015. Geochemical modelling for predicting the long-term performance of zeolite-PRB to treat lead contaminated groundwater. J. Contam. Hydrol. 177, 76–84. https://doi.org/10.1016/j.jconhyd.2015.03.007.

Obiri-Nyarko, F., Kwiatkowska-Malina, J., Malina, G., Wołowiec, K., 2020. Assessment of zeolite and compost-zeolite mixture as permeable reactive materials for the removal of lead from a model acidic groundwater. J. Contam. Hydrol. 229, 103597 https://doi.org/10.1016/j.jconhyd.2019.103597.

Osagie, E., Owabor, C.N., 2015. Adsorption of benzene in batch system in natural clay and sandy soil. Adv. Chem. Eng. Sci. 5, 352–361. https://doi.org/10.4236/aces.2015.53037.

Özer, A., Pirincci, H.B., 2006. The adsorption of Cd (II) ions on sulphuric acid-treated wheat bran. J. Hazard. Mater. 137, 849–855. https://doi.org/10.1016/j.jhazmat.2006.03.009.

Pang, L., Close, M., Schneider, D., Stanton, G., 2002. Effect of pore-water velocity on chemical nonequilibrium transport of Cd, Zn, and Pb in alluvial gravel columns. J. Contam. Hydrol. 57, 241–258. https://doi.org/10.1016/s0169-7722(01)00223-6.

Parashar, R., Govindaraju, R.S., Hantush, M.M., 2007. Temporal moment analysis for volatile organic compounds in dual-porosity porous media: loss fractions and effective parameters. J. Environ. Eng. 133, 879–890. https://doi.org/10.1061/(ASCE)0733-9372(2007)133:9(879).

Priddle, M.W., Jackson, R.E., 1991. Laboratory column measurement of VOC retardation factors and comparison with field values. Groundwater 29, 260–266. https://doi.org/10.1111/j.1745-6584.1991.tb00518.x.

Rabideau, A.J., Suribhatla, R., Craig, J.R., 2005. Analytical models for the design of iron-based permeable reactive barriers. J. Environ. Eng. 131, 1589–1597. https://doi.org/10.1061/ASCE0733-93722005131:111589.

Richards, L.A., 1968. Diagnosis and Improvement of Saline and Alkali Soils. USDA Handbook, 60. U.S. Government Printing Office, Washington, DC.

Sander, M., Pignatello, J.J., 2009. Sorption irreversibility of 1,4-dichlorobenzene in two natural organic matter–rich geosorbents. Environ. Toxicol. Chem. 28, 447–457. https://doi.org/10.1897/08-128.1.

Selim, H.M., Ma, L., Zhu, H., 1999. Predicting solute transport in soils second-order two-site models. Soil Sci. Soc. Am. J. 63, 768–777. https://doi.org/10.2136/sssaj1999.634768x.

Simantiraki, F., Gidarakos, E., 2015. Comparative assessment of compost and zeolite utilisation for the simultaneous removal of BTEX, Cd and Zn from the aqueous phase: batch and continuous flow study. J. Environ. Manag. 159, 218–226. https://doi.org/10.1016/j.jenvman.2015.04.043.

Simpson, J.A., Bowman, R.S., 2009. Nonequilibrium sorption and transport of volatile petroleum hydrocarbons in surfactant-modified zeolite. J. Contam. Hydrol. 108, 1–11. https://doi.org/10.1016/j.jconhyd.2009.05.001.

Singh, P., Kanwar, R.S., 1991. Preferential solute transport through macropores in large undisturbed saturated soil columns. J. Environ. Qual. 20, 295–300. https://doi.org/10.2134/jeq1991.00472425002000010048x.

Suponik, T., 2010. Adsorption and biodegradation in PRB technology. Environ. Prot. Eng. 36, 43–57. http://epe.pwr.wroc.pl/contents.html.

Sutherland, R.A., 1998. Loss-on-ignition estimates of organic matter and relationships to organic carbon in fluvial bed sediments. Hydrobiologia 389, 153–167. https://doi.org/10.1023/A:1003570219018.

Tan, K.L., Hameed, B.H., 2017. Insight into the adsorption kinetics models for the removal of contaminants from aqueous solutions. J. Taiwan Inst. Chem. Eng. 74, 25–48. https://doi.org/10.1016/j.jtice.2017.01.024.

Thierrin, J., Davis, G.B., Barber, C., 1995. A ground-water tracer test with deuterated compounds for monitoring in situ biodegradation and retardation of aromatic hydrocarbons. Groundwater 33, 469–475. https://doi.org/10.1111/j.1745-6584.1995.tb00303.x.

Thornton, S.F., Bright, M.I., Lerner, D.N., Tellam, J.H., 2000. Attenuation of landfill leachate by UK Triassic sandstone aquifer materials: 2. sorption and degradation of organic pollutants in laboratory columns. J. Contam. Hydrol. 43, 355–383. https://doi.org/10.1016/S0169-7722(99)00105-9.

Thorpe, V.A., 1973. Collaborative study of the cation exchange capacity of peat materials. J. Assoc. Anal. Chem. (AOAC) 56, 154–157. https://doi.org/10.1093/jaoac/56.1.154.

Topp, G.C., 1993. Soil water content. In: Carter, M.R. (Ed.), Soil Sampling and Methods of Analysis. Lewis Publishers, London.

Vaezihir, A., Bayanlou, M.B., Ahmadnezhad, Z., Barzegari, G., 2020. Remediation of BTEX plume in a continuous flow model using zeolite-PRB. J. Contam. Hydrol. 230, 103604 https://doi.org/10.1016/j.jconhyd.2020.103604.

Vidal, C.B., Raulino, G.S., Barros, A.L., Lima, A.C., Ribeiro, J.P., Pires, M.J., Nascimento, R.F., 2012. BTEX removal from aqueous solutions by HDTMA-modified Y zeolite. J. Environ. Manag. 112, 178–185. https://doi.org/10.1016/j.jenvman.2012.07.026.

Vignola, R., Bagatin, R., Alessandra De Folly, D., Flego, C., Nalli, M., Ghisletti, D., Sisto, R., 2011. Zeolites in a permeable reactive barrier (PRB): one year of field experience in a refinery groundwater—part 1: the performances. Chem. Eng. J. 178, 204–209. https://doi.org/10.1016/j.cej.2011.10.052.

Waybrant, K.R., Ptacek, C.J., Blowes, D.W., 2002. Treatment of mine drainage using permeable reactive barriers: column experiments. Environ. Sci. Technol. 36, 1349–1356. https://doi.org/10.1021/es010751g.

Weber, W.J., Morris, J.C., 1963. Kinetics of adsorption on carbon from solution. J. Sanit. Eng. Div. 89, 31–60. https://doi.org/10.1061/JSEDAI.0000430.

Weiner, E.R., 2008. Applications of Environmental Aquatic Chemistry: A Practical Guide, 2nd ed. CRC Press, Taylor and Francis Group, Boca Raton, FL.

Wibowo, N., Setyadhi, L., Wibowo, D., Setiawan, J., Ismadji, S., 2007. Adsorption of benzene and toluene from aqueous solutions onto activated carbon and its acid and heat treated forms: influence of surface chemistry on adsorption. J. Hazard. Mater. 146, 237–242. https://doi.org/10.1016/j.jhazmat.2006.12.011.

Wright, A.L., Yu, W., Reddy, K.R., 2008. Loss-on-ignition method to assess soil organic carbon in Calcareous Everglades wetlands. Commun. Soil Sci. Plant Anal. 39, 3074–3083. https://doi.org/10.1080/00103620802432931.

Yang, H., Hu, R., Ruppert, H., Noubactep, C., 2021. Modeling porosity loss in Fe0-based permeable reactive barriers with Faraday's law. Sci. Rep. 11, 1–13. https://doi.org/10.1038/s41598-021-96599-8.

Zawierucha, I., Nowik-Zajac, A., 2019. Evaluation of permeable sorption barriers for removal of Cd (II) and Zn (II) ions from contaminated groundwater. Water Sci. Technol. 80, 448–457. https://doi.org/10.2166/wst.2019.288.

Zheng, Z., Aagaard, P., Breedveld, G.D., 2002. Sorption and anaerobic biodegradation of soluble aromatic compounds during groundwater transport. 1. laboratory column experiments. Environ. Geol. 41, 922–932. https://doi.org/10.1007/s00254-001-0470-2.